Published in final edited form as:
J Chem Phys. 2006 May 21; 124(19): 194303.

Frequency-selective homonuclear dipolar recoupling in solid state NMR

Anant K. Paravastu and **Robert Tycko***
Laboratory of Chemical Physics, National Institute of Diabetes and Digestive and Kidney Diseases, National Institutes of Health, Bethesda, Maryland 20892-0520

Abstract

We introduce a new approach to frequency-selective homonuclear dipolar recoupling in solid state nuclear magnetic resonance (NMR) with magic-angle spinning (MAS). This approach, to which we give the acronym SEASHORE, employs alternating periods of double-quantum recoupling and chemical shift evolution to produce phase modulations of the recoupled dipole-dipole interactions that average out undesired couplings, leaving only dipole-dipole couplings between nuclear spins with a selected pair of NMR frequencies. In principle, SEASHORE is applicable to systems with arbitrary coupling strengths and arbitrary sets of NMR frequencies. Arbitrary MAS frequencies are also possible, subject only to restrictions imposed by the pulse sequence chosen for double-quantum recoupling. We demonstrate the efficacy of SEASHORE in experimental ^{13}C NMR measurements of frequency-selective polarization transfer in uniformly ^{15}N,^{13}C-labeled L-valine powder and frequency-selective intermolecular polarization transfer in amyloid fibrils formed by a synthetic decapeptide containing uniformly ^{15}N,^{13}C-labeled residues.

Introduction

Recoupling techniques are radio-frequency (rf) pulse sequences applied in synchrony with sample rotation that restore nuclear spin interactions that are otherwise averaged out by magic-angle spinning (MAS). The development of recoupling techniques for chemical shift anisotropy[1–4], homonuclear dipole-dipole couplings[5–14], heteronuclear dipole-dipole couplings[15,16], and scalar couplings[17,18] has revolutionized the application of solid state nuclear magnetic resonance (NMR) to chemically and structurally complex materials, where MAS is generally required to permit spectroscopic resolution of NMR signals from inequivalent sites and to enhance sensitivity. Recoupling techniques allow anisotropic interactions to be measured in the evolution periods of a multidimensional NMR measurement, while preserving the high resolution and high sensitivity afforded by MAS in the signal detection period. Recoupling techniques also permit polarization transfers through dipole-dipole or scalar couplings in mixing periods between evolution and/or detection periods.

In solid state ^{15}N and ^{13}C NMR, dipolar recoupling techniques were originally developed for structural measurements on samples that are isotopically labeled at selected sites, typically a ^{13}C-^{13}C or ^{15}N-^{13}C spin pair. Lately, experiments on samples with numerous isotopic labels have become more common, motivated by the goal of obtaining maximal information from a single sample and by the relative ease of preparing uniformly labeled proteins by expression in bacteria. Measurement of dipolar couplings (and hence inter-nuclear distances) between selected spin pairs in the in the presence of couplings to other spins requires frequency-selective recoupling techniques.

*corresponding author: Dr. Robert Tycko, National Institutes of Health, Building 5, Room 112, Bethesda, MD 20892-0520. phone: 301-402-8272. fax: 301-496-0825. e-mail: robertty@mail.nih.gov..

In the case of heteronuclear dipolar recoupling, Jaroniec *et al*. have introduced frequency-selective versions of the rotational echo double resonance (REDOR)[19,20] and transferred echo double resonance (TEDOR) techniques[21] that are effective as long as at least one spin in the pair of interest has a sufficiently well resolved signal under MAS that it can be selectively inverted by a weak π pulse.

In the case of homonuclear dipolar recoupling, frequency-selective techniques have also been proposed[22–25]. These techniques depend on the ability to match the sum or difference of effective fields in the rotating frame for the spin pair of interest to the MAS frequency or a multiple thereof. For good selectivity, the spins to be recoupled must have effective fields in the rotating frame $\nu_{\mathrm{eff}} \equiv \sqrt{\nu_1^2 + \Delta\nu^2}$, where ν_1 is the rf field strength and $\Delta\nu$ is the resonance offset) that are significantly different from those of other spins. In particular, the differences in effective fields must be greater than the dipole-dipole coupling strengths for the undesired spin pairs. These considerations make it difficult to achieve good selectivity unless there are large differences in the resonance offsets, *i.e.*, large chemical shift differences. For aliphatic ^{13}C sites, experimentally relevant chemical shift differences may be in the 5–20 ppm range, corresponding to resonance offset differences in the 0.7–3.0 kHz range in a 14.1 T field, while dipole-dipole coupling constants ($d_{IS} = \gamma^2 \hbar/2\pi R_{IS}^3$ where R_{IS} is the distance between spins I and S) are as large as 2.3 kHz. A further complication is that large differences in effective fields can only be achieved when $\nu_1 \leq |\Delta_\nu|$, which in turn means that low MAS frequencies must be used if selective recoupling is to be achieved for spins with small chemical shift differences.

Previously proposed frequency-selective homonuclear dipolar recoupling techniques[22–25] are extensions of the rotational resonance (RR) effect, in which recoupling occurs in the absence of applied rf fields when the resonance offset difference matches a multiple of the MAS frequency[6,26]. RR itself has been shown to be useful in uniformly labeled samples[27–29], but obviously does not apply when the chemical shift differences are small. The RR matching condition can be broadened in a controlled manner by the application of appropriate amplitude-modulated or phase-modulated rf pulse sequences[30], but this does not eliminate the requirements for large chemical shift differences, weak rf fields, and relatively low MAS frequencies.

In this paper, we describe and demonstrate a new approach to selective homonuclear dipolar recoupling that overcomes the limitations described above. This approach employs pulse sequences in which blocks of nonselective recoupling alternate with blocks of free precession under isotropic chemical shifts. Separation of the recoupling and chemical shift evolution periods eliminates the need for weak rf fields. By adjusting the lengths of the chemical shift evolution periods, selective recoupling can be achieved in principle for arbitrary sets of chemical shift differences. The MAS frequency can also be arbitrarily high, subject only to limitations imposed by the nonselective recoupling technique employed in the recoupling blocks. We refer to this approach to selective homonuclear dipolar recoupling by the acronym SEASHORE (Shift-Evolution-Assisted Selective HOmonuclear REcoupling). In the following sections, we describe the theoretical basis for SEASHORE, present initial demonstrations of selective ^{13}C-^{13}C polarization transfer under SEASHORE in experiments on uniformly ^{15}N,^{13}C-labeled L-valine powder and on an amyloid fibril sample containing uniformly labeled amino acid residues, and discuss likely applications and extensions of SEASHORE.

Theory

As shown in Fig. 1a, the SEASHORE pulse sequence consists of alternating blocks of dipolar recoupling, for time period $m\tau_R$, and chemical shift evolution, for time period $n\tau_R$, where τ_R

is the rotor period and m and n are integers. During the recoupling blocks, the effective Hamiltonian is assumed to include only dipole-dipole coupling terms. In the experiments described below, a double-quantum recoupling technique is used, so the effective Hamiltonian for a pair of spins has the form

$$H_{DQ} = \omega_d I_+ S_+ + \omega_d^* I_- S_- \quad (1)$$

where ω_d is a complex coupling constant with orientation dependence and scaling factor determined by the details of the recoupling technique. During the chemical shift evolution blocks, the effective Hamiltonian has the form

$$H_{CS} = \omega_I I_z + \omega_S S_z \quad (2)$$

where ω_I and ω_S are the resonance offsets for spins I and S. Eq. (2) assumes that the dipole-dipole couplings and chemical shift anisotropy are averaged to zero by MAS during the chemical shift evolution blocks, *i.e.*, that the MAS frequency is large compared with the couplings and that RR conditions are avoided. After N repetitions of double-quantum recoupling and chemical shift evolution blocks, the total evolution operator $U_T(N)$ is

$$U_T(N) = \overbrace{(U_{CS}U_{DQ})(U_{CS}U_{DQ})\ldots(U_{CS}U_{DQ})}^{N\ \text{terms}} \quad (3a)$$

$$= U_{CS}^N (U_{CS}^{-(N-1)} U_{DQ} U_{CS}^{(N-1)})(U_{CS}^{-(N-2)} U_{DQ} U_{CS}^{(N-2)}) \ldots (U_{CS}^{-1} U_{DQ} U_{CS}) U_{DQ} \quad (3b)$$

$$= U_{CS}^N \mathcal{U}_{N-1} \mathcal{U}_{N-2} \cdots \mathcal{U}_1 \mathcal{U}_0 \quad (3c)$$

where

$$U_{DQ} = e^{-imH_{DQ}\tau_R} \quad (4)$$

$$U_{CS} = e^{-inH_{CS}\tau_R} \quad (5)$$

$$\mathcal{U}_M = e^{-im\mathcal{H}_M\tau_R} \quad (6)$$

$$\mathcal{H}_M = \omega_d I_+ S_+ e^{iM\varphi_{IS}} + \omega_d^* I_- S_- e^{-iM\varphi_{IS}} \quad (7)$$

$$\varphi_{IS} = n(\omega_I + \omega_S)\tau_R \quad (8)$$

U_{DQ} and U_{CS} are evolution operators for the double-quantum recoupling and chemical shift evolution blocks, respectively. $\mathcal{U}_M$ is the evolution operator for the M^{th} repetition in an interaction representation with respect to the chemical shifts, with effective Hamiltonian $\mathcal{H}_M$. Phase modulation of $\mathcal{H}_M$, with constant phase increments φ_{IS}, is due to the chemical shift evolution periods and follows from the relation $e^{iI_z\theta} I_+ e^{-iI_z\theta} = e^{i\theta} I_+$. In the limit $\Gamma_d \equiv |m\omega_d\tau_R| << 1$, the approximation

$$U_{N-1}U_{N-2}\cdots U_1U_0 \approx e^{-im\sum_{M=0}^{N-1}H_M\tau_R} \quad (9)$$

is valid. Then, since

$$\sum_{M=0}^{N-1} H_M = \omega_d I_+ S_+ \sum_{M=0}^{N-1} e^{iM\varphi_{IS}} + \omega_d^* I_+ S_+ \sum_{M'=0}^{N-1} e^{-iM'\varphi_{IS}}, \quad (10)$$

phase modulation of H_M will tend to cancel out evolution under the double-quantum recoupling blocks, leading to $U_T(N) \approx U_{CS}^N$, unless φ_{IS} is zero or a multiple of 2π. For a sample with any set of chemical shifts, it is generally possible to find combinations of n, τ_R, and rf carrier frequency such that recoupling occurs for one pair of NMR lines (most simply by setting the carrier frequency to the average of the two NMR frequencies, so that $\omega_I + \omega_S = 0$) and is suppressed for all other pairs of lines. Exact cancellation over N repetitions occurs when $\varphi_{IS} = 2\pi\, k/N$, for integer k satisfying $0 < k < N$, but exact cancellation is not necessarily required for experiments to be successful.

The above arguments are valid for nuclei with arbitrary spin quantum numbers. In the special case of spin-1/2 nuclei, we can use the direct product basis

$$\{|1\rangle \equiv |1/2,\ 1/2\rangle,\ |2\rangle \equiv |1/2,\ -1/2\rangle,\ |3\rangle \equiv |-1/2,\ 1/2\rangle,\ |4\rangle \equiv |-1/2,\ 1/2\rangle\} \quad (11)$$

and the fictitious spin-1/2 operators[31] defined by

$$I_x^{(1,4)} = \frac{1}{2}(|4\rangle\langle 1| + |1\rangle\langle 4|) \quad (12a)$$

$$I_y^{(1,4)} = \frac{i}{2}(|4\rangle\langle 1| - |1\rangle\langle 4|) \quad (12b)$$

$$I_z^{(1,4)} = \frac{1}{2}(|1\rangle\langle 1| - |4\rangle\langle 4|) \quad (12c)$$

to represent H_{DQ} as

$$H_{DQ} = 2[\,\mathrm{Re}(\omega_d) I_x^{(1,4)} - \mathrm{Im}(\omega_d) I_y^{(1,4)}] \quad (13a)$$

$$= 2|\omega_d| I_x^{(1,4)} \quad (13b)$$

where

$$I_x^{(1,4)\prime} = R_z^{(1,4)}(\theta_d) I_x^{(1,4)} R_z^{(1,4)}(-\theta_d) \quad (14a)$$

$$R_z^{(1,4)}(\theta) \equiv e^{-i\theta I_z^{(1,4)}} \quad (14b)$$

$$\theta_d = \arctan\left(\frac{\mathrm{Im}(\omega_d)}{\mathrm{Re}(\omega_d)}\right) \quad (14c)$$

Thus, evolution under H_{DQ} is a nutation of the initial sum magnetization (represented by a density operator term proportional to $I_z^{(1,4)}$) at frequency about the x' axis, which is a vector in the xy plane,. When restricted to the $\{|1\rangle,|4\rangle\}$ subspace, H_{CS} can be written as

$$H_{CS} = (\omega_I + \omega_S)I_z^{(1,4)} \quad (15)$$

According to Eqs. 14 and 15, evolution under SEASHORE can be viewed as an alternating series of rotations about x' by Γ_d and about z by φ_{IS}. When $\Gamma_d \ll 1$ and φ_{IS} is not close to a multiple of 2π, the rotations about $'$ have no net effect, as in the DANTE technique commonly used for frequency selective excitation in NMR[32].

Experimental results

Pulse sequence

Experiments were performed at 9.39 T and room temperature, using a Varian InfinityPlus NMR spectrometer and a Varian 3.2 mm MAS probe. Fig. 1b shows the full pulse sequence used in our initial demonstrations of SEASHORE. ^{13}C spin polarization was first generated by cross polarization (CP) from protons[33] and placed onto the rotating frame z axis by a hard ^{13}C $\pi/2$ pulse. After a short delay τ_1 (100 μs in our experiments), a frequency-selective Gaussian-shaped π pulse (1.2 ms long and applied every second scan with corresponding alternation of the receiver phase) selected signals derived from nuclear magnetization originating at a single ^{13}C site. The subsequent SEASHORE period allowed polarization transfers to proximate ^{13}C sites. After another τ_1 delay, a final hard ^{13}C $\pi/2$ pulse allowed measurement of NMR signals. Continuous wave (cw) proton decoupling was applied during the Gaussian-shaped pulse and SEASHORE periods. Two-pulse phase modulated (TPPM) decoupling[34] was applied during signal detection. Polarization transfer efficiencies consistently improved with increased proton decoupling fields during SEASHORE recoupling blocks, up to the maximum field possible for our NMR probe (150 kHz). For long total recoupling times, it was also advantageous to trigger the beginning of each double-quantum recoupling block with a square wave from the MAS tachometer, to ensure synchronization of the SEASHORE pulse sequence with the sample rotation even in the presence of small instabilities (< 0.05%) in the MAS frequency.

Double-quantum recoupling was achieved with the POST-C7 technique of Hohwy *et al.*[8], with m = 2 (*i.e.*, one full POST-C7 cycle per recoupling block). MAS frequencies of between 6.32 and 9.76 kHz were used, implying ^{13}C rf fields between 44.24 and 68.32 kHz. During the POST-C7 and chemical shift evolution blocks, the ^{13}C rf carrier frequency was set to the average of the NMR frequencies of the two sites to be recoupled, except as described below for Fig. 3. Values of n and τ_R were chosen to suppress the recoupling of dipole-dipole interactions involving other sites, according to the principles described above.

Selective polarization transfers within uniformly ^{13}C-labeled valine

Fig. 2 demonstrates the efficacy of SEASHORE in experiments on uniformly ^{15}N,^{13}C-labeled L-valine powder. The conventional ^{13}C MAS NMR spectrum is shown in Fig. 2a. The remaining spectra were obtained with the pulse sequence in Fig. 1b. Fig. 2b shows the spectrum obtained with initial selection of C_α spin polarization and subsequent recoupling for 2.286 ms without chemical shift evolution blocks (*i.e.*, n = 0). These conditions lead to recoupling of dipole-dipole interactions between all ^{13}C spins, and therefore to transfer from C_α to all other carbon sites. The double-quantum nature of POST-C7 recoupling leads to alternating signs for NMR lines of spins that are polarized primarily by a series of single-bond transfers. In particular, the $C_{\gamma 2}$ NMR line is positive in Fig. 2b because it results primarily from two single-bond polarization transfers from C_α. Fig. 2c shows the spectrum obtained with initial selection

of the C_α spin polarization and subsequent SEASHORE recoupling of the C_α-$C_{\gamma 2}$ interaction, with n = 3 and N = 14 (3.841 ms of POST-C7, 9.605 ms total recoupling time). The $C_{\gamma 2}$ NMR line is negative in Fig. 2c, indicating that this line results from direct polarization transfer between ^{13}C sites that are separated by two bonds. All other transfers are suppressed, except for a weak transfer to $C_{\gamma 1}$ due to the small chemical shift difference between $C_{\gamma 1}$ and $C_{\gamma 2}$ NMR lines, even though C_α-C_β and C_α-CO dipole-dipole couplings are approximately 4.4 times stronger than C_α-$C_{\gamma 1}$ and C_α-$C_{\gamma 2}$ couplings. Fig. 2d shows the spectrum obtained with initial selection of the CO spin polarization and subsequent SEASHORE recoupling of the CO-$C_{\gamma 2}$ interaction, with n = 4 and N = 26 (7.560 ms of POST-C7, 22.601 ms total recoupling time). Again, the $C_{\gamma 2}$ NMR line is negative in Fig. 2d and all other transfers are strongly suppressed, indicating selective recoupling of the CO-$C_{\gamma 2}$ interaction and direct polarization transfer from CO to $C_{\gamma 2}$, separated by three bonds.

Fig. 3 shows the effects of varying the ^{13}C rf carrier frequency away from its optimal value for C_α-$C_{\gamma 2}$ recoupling, which is the average of the C_α and $C_{\gamma 2}$ NMR frequencies. Plotted are the integrated intensities of the CO, C_β, $C_{\gamma 1}$, and $C_{\gamma 2}$ NMR lines as functions of the offset from the optimal carrier frequency. Pulse sequence parameters were optimized for suppression of all undesired transfers at the optimal carrier frequency. Deviation from the optimal carrier frequency results in loss of the desired transfer and growth of undesired transfers. The strongest undesired transfer is from C_α to $C_{\gamma 1}$, which is maximized as expected when the carrier frequency equals the average of the C_α and $C_{\gamma 1}$ NMR frequencies, marked by the vertical dashed line in Fig. 3.

Time dependence of selective polarization transfers

Fig. 4 demonstrates the selective measurement of internuclear distances in uniformly ^{15}N,^{13}C-labeled L-valine powder, through the dependence of frequency-selective polarization transfers on the total recoupling time in the SEASHORE sequence. We quantify polarization transfer by the value of $(F_i + F_j)/(F_i - F_j)$, where F_i and F_j are peak integrals proportional to longitudinal spin angular momenta of spins *i* and *j*, respectively, immediately after the SEASHORE recoupling period. The normalizing factor $(F_i - F_j)$ is included to account partially for loss of signal due to transverse nuclear relaxation during the SEASHORE period, and would be time-independent in the limit of pure double-quantum evolution without relaxation.

As shown in Fig. 4a, frequency-selective polarization transfer from C_β to $C_{\gamma 2}$ exhibits a damped oscillatory time dependence, with stronger damping at lower proton decoupling fields. Comparison with the oscillations in simulated curves, calculated for a two-spin system under ideal POST-C7 pulse sequence conditions, indicates a distance of 1.50 ± 0.05 Å. The true C_β-$C_{\gamma 2}$ distance is 1.53 Å, according to the crystal structure of L-valine[35], which contains two inequivalent L-valine molecules in the unit cell. As shown in Fig. 4b, frequency-selective polarization transfer from C_α to $C_{\gamma 2}$ also exhibits a damped oscillatory time dependence. Comparison with simulated curves indicates a distance of 2.50 ± 0.05 Å. Distances from C_α sites to C_γ sites in the crystal structure range from 2.53 Å to 2.56 Å.

As shown in Fig. 4c, frequency-selective polarization transfer from CO to $C_{\gamma 2}$ is weakly oscillatory. The normalized polarization transfer does not decay to zero. We attribute this observation to the fact that the CO and $C_{\gamma 2}$ NMR lines are actually superpositions of lines with small, unresolved chemical shift differences, arising from the two inequivalent molecules in the L-valine crystal structure. Given the relatively long internuclear distances and weak dipole-dipole couplings for CO-$C_{\gamma 2}$ pairs, complete polarization transfer may then be prevented by small offsets from the exact condition $\omega_I + \omega_S = 0$ (see below). Simulated curves in Fig. 4c are for the four distinct intramolecular distances between CO and C_γ sites in crystalline L-valine. The assignment of $C_{\gamma 1}$ and $C_{\gamma 2}$ lines to specific C_γ sites is not known. Two-dimensional solid

state NMR spectra of uniformly ^{15}N,^{13}C-labeled L-valine powder (data not shown) indicate that both inequivalent L-valine molecules contribute to the $C_{\gamma 2}$ line, implying four pairs of internuclear distances that may be assigned to CO-$C_{\gamma 2}$ distances[35]: 2.90 Å and 2.98 Å; 2.98 Å and 3.29 Å; 2.90 Å and 3.90 Å; 3.29 Å and 3.90 Å. The experimental data in Fig. 4c appear more consistent with the first two possible assignments.

All simulated curves in Fig. 4 include artificial damping with a 5 ms time constant to produce approximate agreement with the experimental data. One important source of damping in experimental data is imperfect proton decoupling, as the oscillations in Fig. 4 increase in amplitude when the proton decoupling fields during POST-C7 blocks are increased from 110 kHz to 150 kHz. Inhomogeneity of rf fields may also contribute to the damping of oscillatory polarization transfers. To address this issue, simulations were performed for a two-spin system with a 1.50 Å internuclear distance, τ_R = 100 μs, m = 2, n = 1, and rf field amplitudes ranging from 0.85 to 1.15 times the ideal value for POST-C7 recoupling, in increments of 0.01. Summation of the simulated curves, with equal weighting, produced a curve with an apparent damping time constant of approximately 5 ms.

Application to amyloid fibrils

Fig. 5 shows an initial application of the SEASHORE technique to a system of genuine biochemical complexity, namely a 6 mg sample of lyophilized amyloid fibrils formed by residues 14–23 of the full-length β-amyloid peptide associated with Alzheimer's disease ($A\beta_{14–23}$, amino acid sequence HQKLFVVAED), synthesized with uniform ^{15}N and ^{13}C labeling of Val18 and Ala21[36]. Determination of the molecular structures of amyloid fibrils formed by various peptides and proteins is an area of current activity in several solid state NMR groups[37–46]. Earlier measurements on $A\beta_{14–23}$ fibrils, using proton-mediated two-dimensional ^{13}C NMR exchange spectroscopy[45,47], had shown that these fibrils contain highly ordered antiparallel β-sheets in which intermolecular hydrogen bonds connect residue 16+j of each $A\beta_{14–23}$ molecule with residue 23-j of a neighboring molecule (data not shown). Thus, Val18 and Ala21 are aligned in the antiparallel β-sheets, producing nearest-neighbor intermolecular distances of approximately 4.2 ± 0.3 Å between C_α of Val18 and C_α of Ala21. The corresponding intramolecular distance is greater than 10 Å, so that any observed polarization transfers must be primarily intermolecular in nature.

Fig. 5a shows the conventional ^{13}C MAS NMR spectrum of the $A\beta_{14–23}$ fibril sample. Fig. 5b shows a spectrum obtained with initial selection of the Ala21 C_α spin polarization and subsequent polarization transfer with SEASHORE under conditions chosen to recouple the intermolecular, inter-residue C_α-C_α dipole-dipole interactions while suppressing all other couplings involving the C_α sites (N = 32, n = 1, 8.392 ms of POST-C7, 12.589 ms total recoupling time, ^{13}C rf carrier at the average of the Ala21 C_α and Val18 C_α NMR frequencies). Although intra-residue C_α-CO and C_α-C_β polarization transfers are not completely eliminated, they are strongly attenuated. Moreover, the desired intermolecular C_α-C_α polarization transfer in Fig. 5b is stronger than the intra-residue transfers, despite the fact that the intermolecular C_α-C_α dipole-dipole coupling is roughly 20 times weaker than the intra-residue couplings. Fig. 5c shows a spectrum obtained under identical conditions, except that the ^{13}C rf carrier frequency during the SEASHORE period is shifted by 1000 Hz. Undesired transfers increase at the expense of the desired intermolecular polarization transfer. The small positive signal at the Val18 C_α chemical shift in Fig. 5c is attributable to weak off-resonance excitation by the Gaussian-shaped pulse. Fig. 5d shows the difference between spectra in Figs. 5b and 5c. The negative sign of the signal at the Val18 C_α NMR frequency in Fig. 5d, together with the absence of Val18 CO and C_β signals, shows that this signal is not an artifact of spectrometer instability, spin relaxation, imperfect phase cycling, or other effects. The integrated Val18 C_α signal camplitude in Fig. 5b is 1.4% and 3.6% of the A21 C_α signal amplitudes in Figs. 5a and 5b,

respectively. Assuming a 4.2 Å internuclear distance, the ideal polarization transfer efficiency under the conditions in Fig. 5b would be 21%. For comparison, proton-mediated C_α-C_α polarization transfers have efficiencies of roughly 5–10% in antiparallel β-sheet structures under experimental conditions used for structural measurements[45,47].

Discussion

We envision many applications of SEASHORE in structural studies of solids, including organic, inorganic, and biochemical materials. Of immediate interest to us are structural studies of amyloid fibrils[37–46], integral membrane proteins[48–54], and peptides bound to antibodies or receptor proteins[29,55]. In systems such as these, samples with multiple uniformly ^{15}N,^{13}C-labeled residues are prepared to enable efficient measurements of ^{13}C NMR chemical shifts, from which secondary structure elements are identified. Rough estimates of ^{13}C-^{13}C distances in these samples, which are needed for the development of full structural models, can be obtained from two-dimensional ^{13}C-^{13}C NMR exchange spectroscopy with long exchange periods[56] or from proton-mediated two-dimensional ^{13}C-^{13}C NMR exchange spectroscopy[57], but more quantitative measurements of pairwise ^{13}C-^{13}C distances with SEASHORE would permit structures to be determined with greater detail and precision.

At present, the maximum distances measurable with good precision by SEASHORE are limited by damping of oscillations in the time-dependent polarization transfer curves. When these oscillations are overdamped, internuclear distances can not be measured precisely without a detailed analysis of spin relaxation processes. As demonstrated in Fig. 4a, oscillations were less strongly damped when the proton decoupling field amplitudes during SEASHORE recoupling periods were increased from 110 kHz to 150 kHz. It is likely that proton decoupling fields above 150 kHz would further improve the polarization transfer data. Inhomogeneity of the ^{13}C rf field amplitude across the sample volume is also a contributing factor, as oscillations were less strongly damped when the 10 mg sample used in Fig. 4 was replaced with a 2 mg sample (data not shown).

The SEASHORE technique is also sensitive to inhomogeneous broadening of the ^{13}C MAS NMR lines in a manner similar to other frequency-selective techniques, such as RR[6,26–30]. If the dipole-dipole couplings for the spin pairs of interest are small compared with the inhomogeneous linewidths in the MAS spectrum, as will be the case for measurements of relatively large internuclear distances in noncrystalline samples, then recoupling under SEASHORE will tend to be suppressed. This is true because a weak coupling necessitates a long recoupling period, which in turn implies a narrow recoupling bandwidth. Some of the spin pairs of interest will then be outside the recoupling bandwidth. This effect reduces the Val18 C_α signal amplitude in the experiments on $A\beta_{14–23}$ fibrils in Fig. 5b. In these experiments, the relevant coupling strength is approximately 100 Hz and the inhomogeneous ^{13}C NMR linewidths are approximately 200 Hz. In Fig. 4c, the experimental polarization transfer is also limited by a narrow recoupling bandwidth.

In principle, the recoupling bandwidth under SEASHORE can be increased by the insertion of hard ^{13}C π pulses into the SEASHORE pulse sequence, with a spacing comparable to the inverse of the inhomogeneous linewidths[58]. We are currently exploring this possibility.

Recoupling sequences other than POST-C7 can be incorporated into SEASHORE, including pulse sequences that produce zero-quantum effective dipole-dipole couplings[12–14,17,18]. For example, if the effective couplings have the zero-quantum form

$$H_{ZQ} = \omega_d(3I_zS_z - \boldsymbol{I}\cdot\boldsymbol{S}) \quad (16)$$

then chemical shift differences will average the couplings to the form

$$\mathcal{H}_{ZQ} = 2\omega_d I_z S_z \tag{17}$$

unless $n(\omega_I - \omega_S)\tau_R$ is an integer multiple of 2π. With the form in Eq. (17), all homonuclear dipole-dipole couplings commute with one another and with resonance offsets. Among other reasons, this property is useful because it allows homonuclear dipole-dipole couplings to be refocused by frequency-selective π pulses.

Independently, Chan and coworkers have shown that the introduction of chemical shift evolution periods into the R-TOBSY recoupling sequence leads to frequency-selective polarization transfers[59]. R-TOBSY produces a scalar, zero-quantum effective coupling Hamiltonian[18]. Chemical shift precession produces a phase modulation that truncates the effective Hamiltonian to the form in Eq. (17) unless $n(\omega_I - \omega_S)\tau_R$ is an integer multiple of 2π.

Acknowledgements

This work was supported by the Intramural Research Program of the National Institute of Diabetes and Digestive and Kidney Diseases of the National Institutes of Health, and by a grant to R.T. from the NIH Intramural AIDS Targeted Antiviral Program. We thank Dr. David J. E. Callaway for providing the $A\beta_{14-23}$ sample used in this work. The analogy between SEASHORE and DANTE was suggested to us by Dr. G. Bodenhausen.

References

1. Alla MA, Kundla EI, Lippmaa ET. Jetp Lett 1978;27:194.
2. Tycko R, Dabbagh G, Mirau PA. J Magn Reson 1989;85:265.
3. Chan JCC, Tycko R. J Chem Phys 2003;118:8378.
4. Liu SF, Mao JD, Schmidt-Rohr K. J Magn Reson 2002;155:15. [PubMed: 11945029]
5. Meier BH, Earl WL. J Chem Phys 1986;85:4905.
6. Meier BH, Earl WL. J Am Chem Soc 1987;109:7937.
7. Tycko R, Dabbagh G. Chem Phys Lett 1990;173:461.
8. Hohwy M, Jakobsen HJ, Eden M, Levitt MH, Nielsen NC. J Chem Phys 1998;108:2686.
9. Brinkmann A, Eden M, Levitt MH. J Chem Phys 2000;112:8539.
10. Carravetta M, Eden M, Zhao X, Brinkmann A, Levitt MH. Chem Phys Lett 2000;321:205.
11. Gregory DM, Mitchell DJ, Stringer JA, Kiihne S, Shiels JC, Callahan J, Mehta MA, Drobny GP. Chem Phys Lett 1995;246:654.
12. Gullion T, Vega S. Chem Phys Lett 1992;194:423.
13. Bennett AE, Ok JH, Griffin RG, Vega S. J Chem Phys 1992;96:8624.
14. Ishii Y. J Chem Phys 2001;114:8473.
15. Oas TG, Griffin RG, Levitt MH. J Chem Phys 1988;89:692.
16. Gullion T, Schaefer J. J Magn Reson 1989;81:196.
17. Baldus M, Meier BH. J Magn Reson Ser A 1996;121:65.
18. Chan JCC, Brunklaus G. Chem Phys Lett 2001;349:104.
19. Bennett AE, Becerra LR, Griffin RG. J Chem Phys 1994;100:812.
20. Jaroniec CP, Tounge BA, Herzfeld J, Griffin RG. J Am Chem Soc 2001;123:3507. [PubMed: 11472123]
21. Jaroniec CP, Filip C, Griffin RG. J Am Chem Soc 2002;124:10728. [PubMed: 12207528]
22. Takegoshi K, Nomura K, Terao T. Chem Phys Lett 1995;232:424.
23. Takegoshi K, Nomura K, Terao T. J Magn Reson 1997;127:206. [PubMed: 9281485]
24. Costa PR, Sun BQ, Griffin RG. J Am Chem Soc 1997;119:10821.
25. Ladizhansky V, Griffin RG. J Am Chem Soc 2004;126:948. [PubMed: 14733572]
26. Raleigh DP, Levitt MH, Griffin RG. Chem Phys Lett 1988;146:71.

27. Williamson PTF, Verhoeven A, Ernst M, Meier BH. J Am Chem Soc 2003;125:2718. [PubMed: 12603160]
28. Petkova AT, Tycko R. J Magn Reson 2004;168:137. [PubMed: 15082259]
29. Sharpe S, Kessler N, Anglister JA, Yau WM, Tycko R. J Am Chem Soc 2004;126:4979. [PubMed: 15080704]
30. Chan JCC, Tycko R. J Chem Phys 2004;120:8349. [PubMed: 15267757]
31. Vega S. J Chem Phys 1978;68:5518.
32. Morris GA, Freeman R. J Magn Reson 1969;29:433.
33. Pines A, Gibby MG, Waugh JS. J Chem Phys 1973;59:569.
34. Bennett AE, Rienstra CM, Auger M, Lakshmi KV, Griffin RG. J Chem Phys 1995;103:6951.
35. Torii K, Iitaka Y. Acta Crystallographica Section B-Structural Crystallography and Crystal Chemistry 1970;B 26:1317.
36. Tjernberg LO, Tjernberg A, Bark N, Shi Y, Ruzsicska BP, Bu ZM, Thyberg J, Callaway DJE. Biochem J 2002;366:343. [PubMed: 12023906]
37. Lansbury PT, Costa PR, Griffiths JM, Simon EJ, Auger M, Halverson KJ, Kocisko DA, Hendsch ZS, Ashburn TT, Spencer RGS, Tidor B, Griffin RG. Nat Struct Biol 1995;2:990. [PubMed: 7583673]
38. Benzinger TLS, Gregory DM, Burkoth TS, Miller-Auer H, Lynn DG, Botto RE, Meredith SC. Proc Natl Acad Sci U S A 1998;95:13407. [PubMed: 9811813]
39. Jaroniec CP, MacPhee CE, Bajaj VS, McMahon MT, Dobson CM, Griffin RG. Proc Natl Acad Sci U S A 2004;101:711. [PubMed: 14715898]
40. Kammerer RA, Kostrewa D, Zurdo J, Detken A, Garcia-Echeverria C, Green JD, Muller SA, Meier BH, Winkler FK, Dobson CM, Steinmetz MO. Proc Natl Acad Sci U S A 2004;101:4435. [PubMed: 15070736]
41. Siemer AB, Ritter C, Ernst M, Riek R, Meier BH. Angew Chem-Int Edit 2005;44:2441.
42. Antzutkin ON, Balbach JJ, Leapman RD, Rizzo NW, Reed J, Tycko R. Proc Natl Acad Sci U S A 2000;97:13045. [PubMed: 11069287]
43. Balbach JJ, Ishii Y, Antzutkin ON, Leapman RD, Rizzo NW, Dyda F, Reed J, Tycko R. Biochemistry 2000;39:13748. [PubMed: 11076514]
44. Petkova AT, Ishii Y, Balbach JJ, Antzutkin ON, Leapman RD, Delaglio F, Tycko R. Proc Natl Acad Sci U S A 2002;99:16742. [PubMed: 12481027]
45. Petkova AT, Buntkowsky G, Dyda F, Leapman RD, Yau WM, Tycko R. J Mol Biol 2004;335:247. [PubMed: 14659754]
46. Chan JCC, Oyler NA, Yau WM, Tycko R. Biochemistry 2005;44:10669. [PubMed: 16060675]
47. Tycko R, Ishii Y. J Am Chem Soc 2003;125:6606. [PubMed: 12769550]
48. Hiller M, Krabben L, Vinothkumar KR, Castellani F, van Rossum BJ, Kuhlbrandt W, Oschkinat H. Chembiochem 2005;6:1679. [PubMed: 16138308]
49. van Gammeren AJ, Hulsbergen FB, Hollander JG, de Groot HJM. J Biomol NMR 2005;31:279. [PubMed: 15928995]
50. Patel AB, Crocker E, Reeves PJ, Getmanova EV, Eilers M, Khorana HG, Smith SO. J Mol Biol 2005;347:803. [PubMed: 15769471]
51. Tian CL, Gao PF, Pinto LH, Lamb RA, Cross TA. Protein Sci 2003;12:2597. [PubMed: 14573870]
52. Isaac B, Gallagher GJ, Balazs YS, Thompson LK. Biochemistry 2002;41:3025. [PubMed: 11863441]
53. Ma C, Marassi FM, Jones DH, Straus SK, Bour S, Strebel K, Schubert U, Oblatt-Montal M, Montal M, Opella SJ. Protein Sci 2002;11:546. [PubMed: 11847278]
54. Zysmilich MG, McDermott A. Proc Natl Acad Sci U S A 1996;93:6857. [PubMed: 11607689]
55. Luca S, White JF, Sohal AK, Filippov DV, van Boom JH, Grisshammer R, Baldus M. Proc Natl Acad Sci U S A 2003;100:10706. [PubMed: 12960362]
56. Castellani F, van Rossum BJ, Diehl A, Rehbein K, Oschkinat H. Biochemistry 2003;42:11476. [PubMed: 14516199]
57. Lange A, Becker S, Seidel K, Giller K, Pongs O, Baldus M. Angew Chem-Int Edit 2005;44:2089.
58. Goobes G, Boender GJ, Vega S. J Magn Reson 2000;146:204. [PubMed: 10968974]
59. Mou Y, Chan JCC. Chem Phys Lett 2006;419:144.

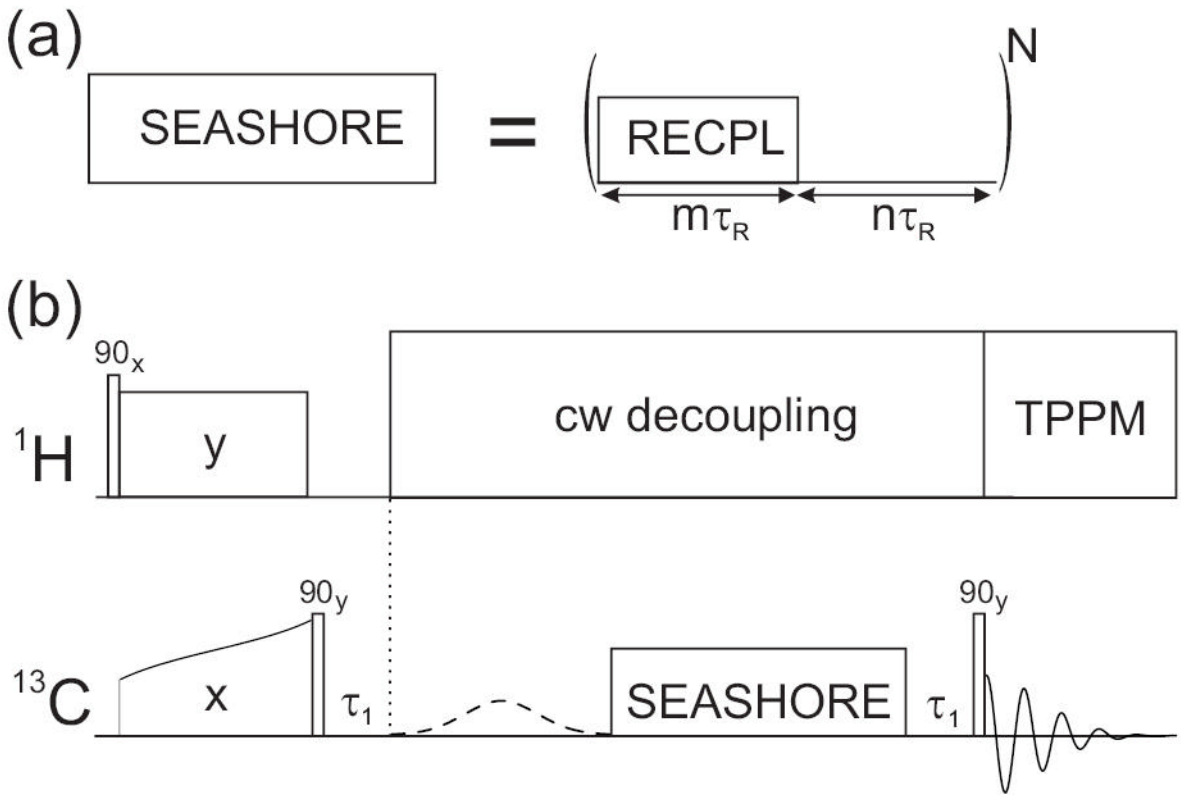

Figure 1.

Pulse sequences for frequency-selective homonuclear dipolar recoupling. (a) The SEASHORE sequence consists of N alternating blocks of dipolar recoupling (RECPL) and chemical shift evolution for multiples of the MAS period τ_R. (b) For demonstrations of frequency-selective spin polarization transfer in solid state ^{13}C NMR in Figs. 2–5, ^{13}C polarization was generated by cross polarization from ^1H spins. After storage as longitudinal magnetization for τ_1, the polarization of a single 13C site was selected by a Gaussian-shaped pulse present every second scan, and transferred under the SEASHORE sequence. ^{13}C NMR signals were detected with TPPM ^1H decoupling, with receiver phase alternation corresponding to the presence or absence of the Gaussian-shaped pulse.

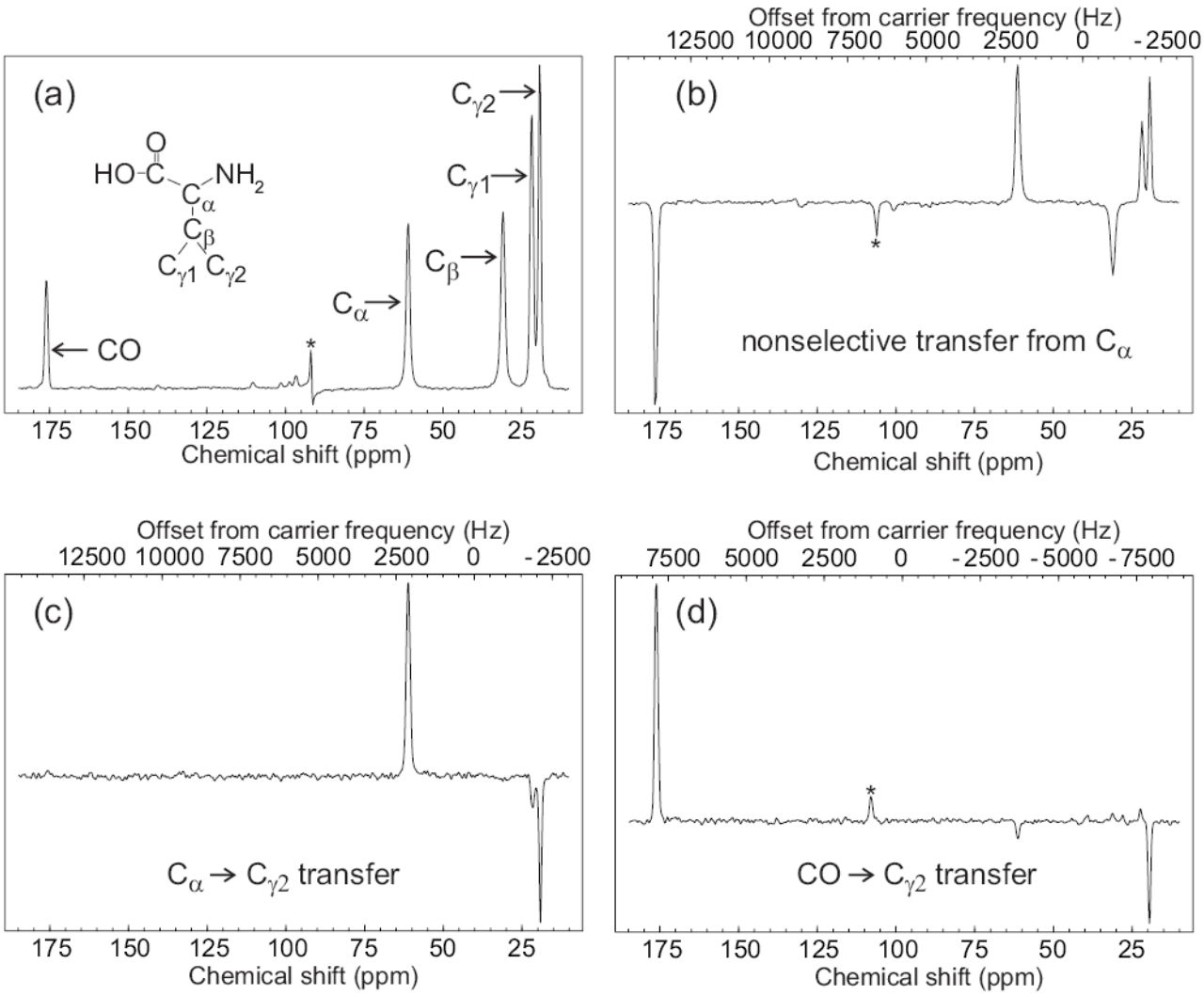

Figure 2.

Demonstration of frequency-selective polarization transfer in uniformly ^{15}N,^{13}C-labeled L-valine powder under SEASHORE, using the POST-C7 recoupling technique. (a) Conventional ^{13}C NMR spectrum with peak assignments, obtained at 100.4 MHz ^{13}C NMR frequency with 8.000 kHz MAS. (b) Spectrum obtained with the pulse sequence in Fig. 1, with selective excitation of the C_α peak, N = 8, m = 2, n = 0, and 7.000 kHz MAS. (c) Spectrum obtained with selective excitation of the C_α peak, N = 14, m = 2, n = 3, and 7.288 kHz MAS. (d) Spectrum obtained with selective excitation of the CO peak, N = 26, m = 2, n = 4, and 6.878 kHz MAS. All spectra were obtained with 16 scans at 100.4 MHz ^{13}C NMR frequency, using a 10 mg sample, and 110 kHz proton decoupling throughout the Gaussian-shaped pulse, SEASHORE recoupling, and signal acquisition. For parts c and d, rf carrier frequencies during the SEASHORE period were set to the midpoint of the ^{13}C NMR frequencies of the spin pair of interest. Values of n and the MAS frequency were chosen to optimize the selectivity of dipolar recoupling. Asterisks indicate an artifact at the carrier frequency in part a and MAS sideband lines in parts b and c.

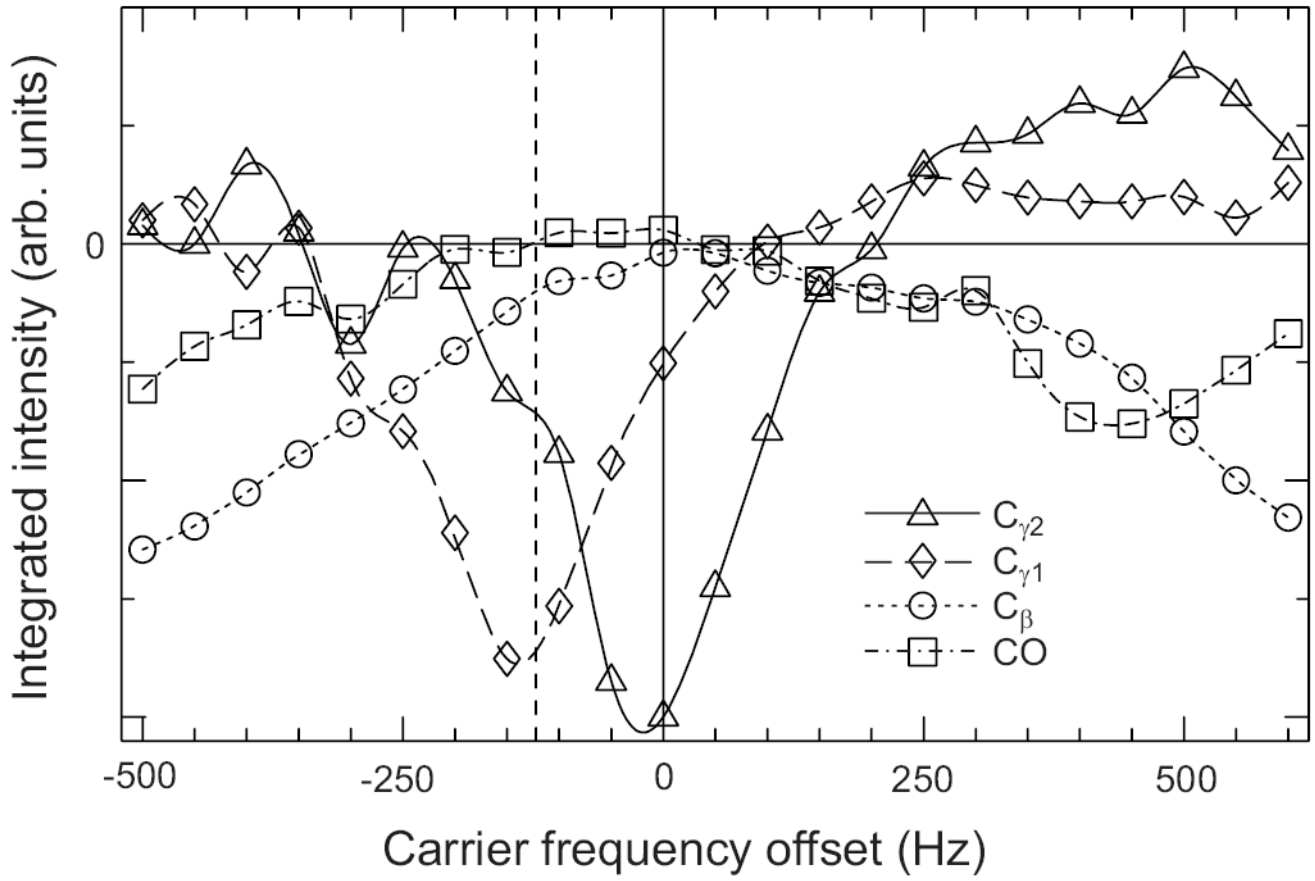

Figure 3.

Dependence of polarization transfers under SEASHORE on the rf carrier frequency. Data are for uniformly ^{15}N,^{13}C-labeled L-valine powder. Experimental parameters other than the carrier frequency are as in Fig. 2c. Carrier frequency offset of zero corresponds to the midpoint of the C_{α} and $C_{\gamma 2}$ NMR frequencies, where conditions were optimized for selective recoupling of C_{α} and $_{\gamma 2}$. Vertical dashed line marks the midpoint of the C_{α} and $C_{\gamma 1}$ NMR frequencies. Lines through the data points are guides to the eye.

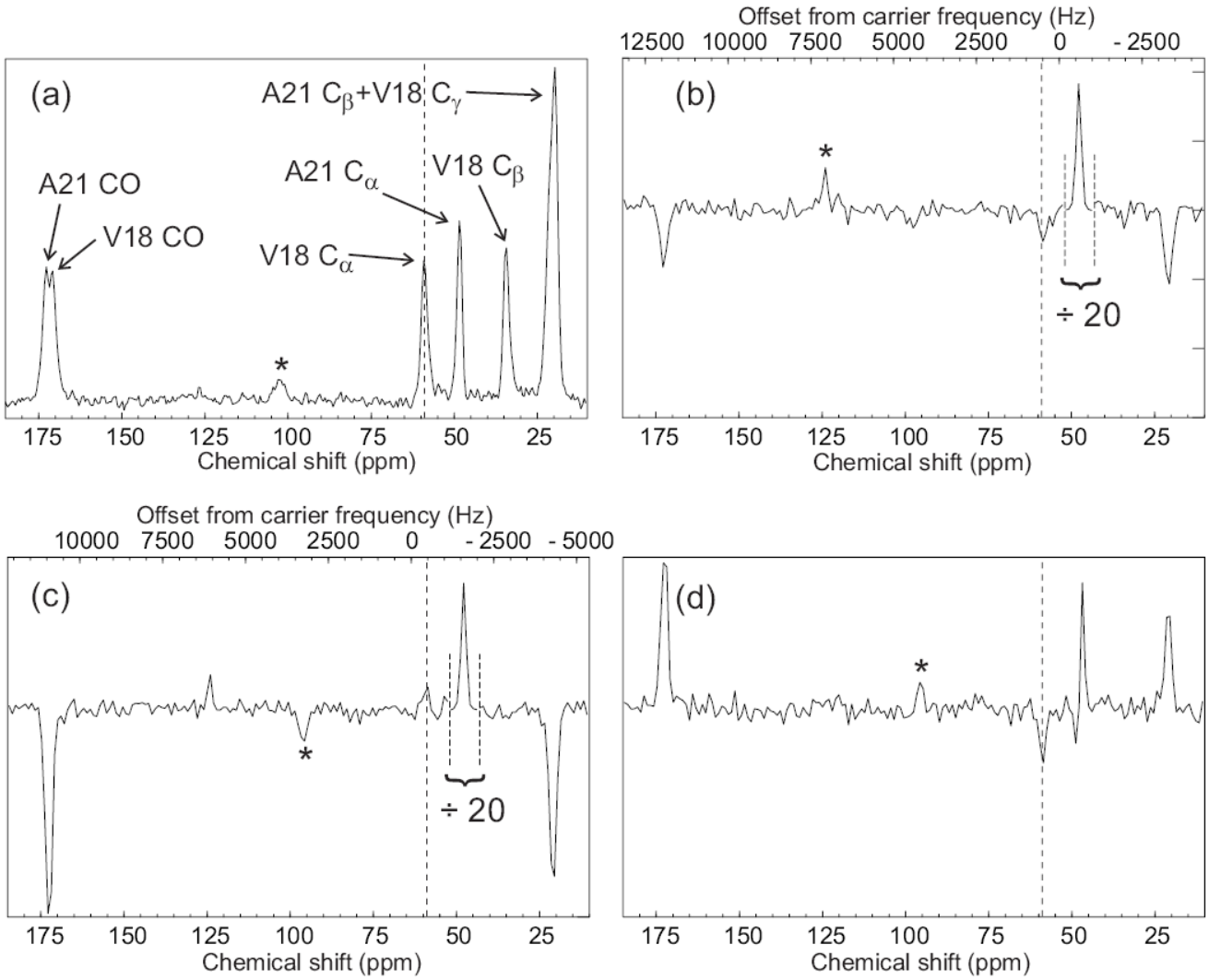

Figure 4.

The dependences of selective double-quantum polarization transfers on the total time of POST-C7 recoupling. Data in parts a, b, and c are for selective C_β-$C_{\gamma 2}$ (filled and hollow triangles), C_α-$C_{\gamma 2}$ (filled squares), and CO-$C_{\gamma 2}$ (filled diamonds) transfers in uniformly ^{15}N,^{13}C-labeled L-valine powder. MAS frequencies were 8.45 kHz, 6.32 kHz, and 9.76 kHz, respectively. Polarization transfers are quantified by $(F_i + F_j)/(F_i - F_j)$, as explained in the text. Peak integrals F_i and F_j were extracted from NMR spectra obtained in 100 scans. Proton decoupling field amplitudes during POST-C7 blocks were 150 kHz (all filled symbols) or 110 kHz (hollow triangles). POST-C7 blocks were actively synchronized with an MAS tachometer signal. Decoupling fields were 110 kHz during the Gaussian-shaped pulse, chemical shift evolution periods, and signal acquisition. Simulated curves are for two-spin systems with the indicated internuclear distances, under ideal pulse sequence conditions. Exponential damping with a 5 ms time constant is applied to all simulated curves.

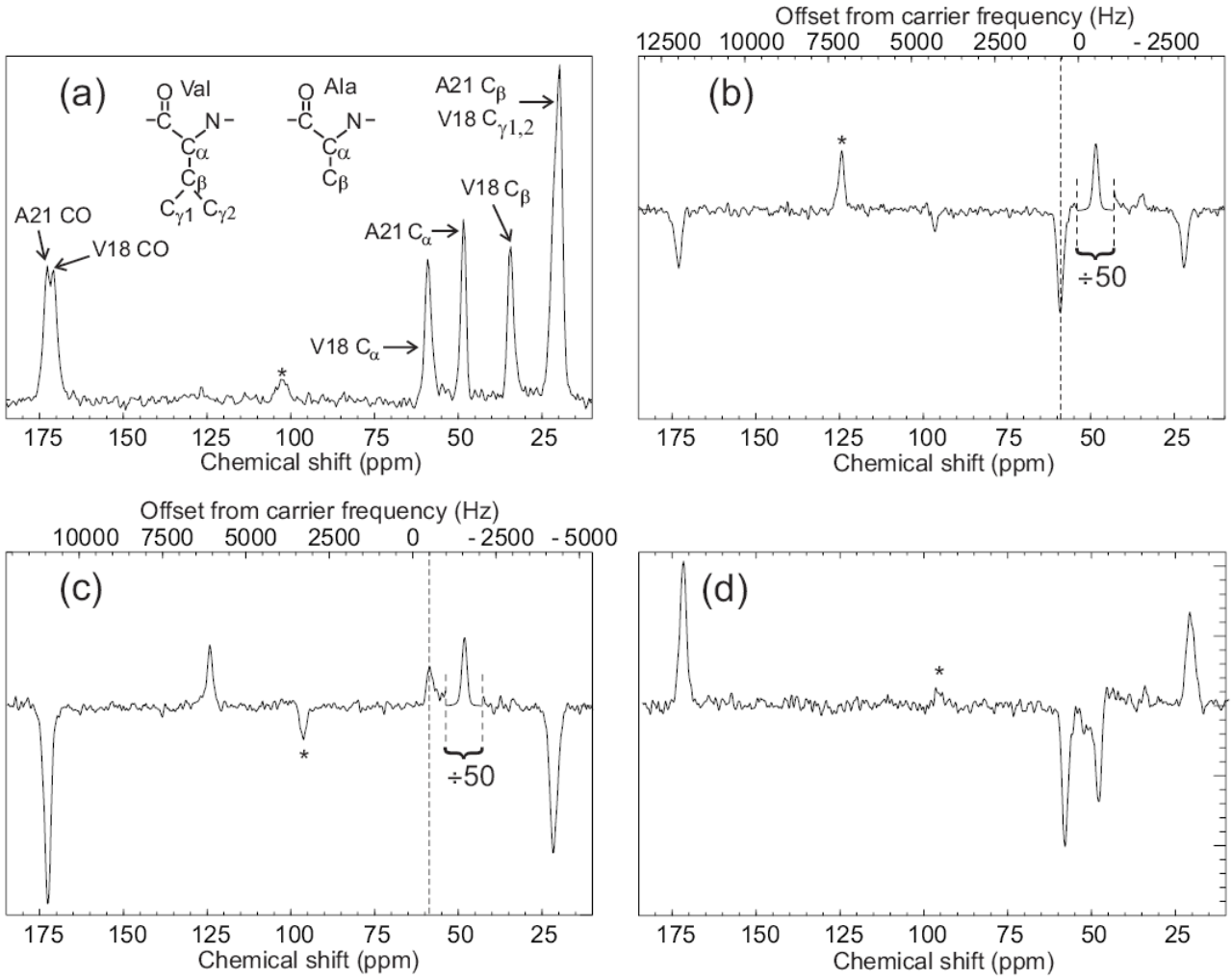

Figure 5.

Observation of an intermolecular polarization transfer between $A\beta_{14–23}$ peptide molecules within amyloid fibrils using SEASHORE. $A\beta_{14–23}$ molecules were uniformly ^{15}N,^{13}C-labeled at Val18 and Ala21. (a) Conventional ^{13}C NMR spectrum with peak assignments, obtained at 100.4 MHz ^{13}C NMR frequency in 16 scans with 7.00 kHz MAS. (b) Spectrum obtained with the pulse sequence in Fig. 1, with selective excitation of the Ala21 C_α peak, N = 32, m = 2, n = 1, and 7.626 kHz MAS. The rf carrier frequency was set to the midpoint of the Ala21 C_α and Val18 C_α NMR frequencies. This spectrum is the result of 50,000 scans. The Ala21 C_α peak is scaled down by a factor of 50 relative to the rest of the spectrum. Vertical dashed line marks the Val18 C_α NMR frequency. (c) Spectrum obtained as in part b, but with a 1000 Hz shift of the carrier frequency during the SEASHORE period to prevent Ala21-Val18 recoupling. (d) The difference of spectra in parts b and c. Asterisks indicate MAS sideband lines.